Hierarchically controlled ecological life support systems

Ciurans, Carles; Bazmohammadi, Najmeh; Poughon, Laurent; Vasquez, Juan C.; Dussap, Claude G.; Gòdia, Francesc; Guerrero, Josep M.

Published in:
Computers and Chemical Engineering

DOI (link to publication from Publisher):
10.1016/j.compchemeng.2021.107625

Publication date:
2022

Document Version
Publisher's PDF, also known as Version of record

Computers and Chemical Engineering 157 (2022) 107625

Contents lists available at ScienceDirect

Computers and Chemical Engineering

journal homepage: www.elsevier.com/locate/compchemeng

Hierarchically controlled ecological life support systems

Carles Ciurans[a,b,*], Najmeh Bazmohammadi[c], Laurent Poughon[b], Juan C. Vasquez[c], Claude G. Dussap[b], Francesc Gòdia[a], Josep M. Guerrero[c]

[a] MELiSSA Pilot Plant-Claude Chipaux Laboratory, Escola de d'Enginyeria, Universitat Autònoma de Barcelona, Carrer de les Sitges, Cerdanyola del Vallès, Spain
[b] Institut Pascal, Campus Universitaire des Cézeaux, 4 Avenue Blaise Pascal, 63178 Aubière, France
[c] Centre for Research on Microgrids (CROM), Aalborg University, AAU Energy, Denmark

ARTICLE INFO

Article history:
Received 4 June 2021
Revised 11 November 2021
Accepted 2 December 2021
Available online 5 December 2021

Keywords:
Hierarchical control structure
Controlled ecological life support systems
Model Predictive Control
Optimization Problem
MELiSSA Pilot Plant

ABSTRACT

Life support systems (LSSs) are autonomous systems integrating various generation, recycling, and consumption subsystems with storage capability to maintain the balance of key system compounds. A novel hierarchical control is proposed in this paper to operate an exemplary controlled ecological LSS. The study focuses on the control of O_2 concentration in the crew compartment, as the main consumer of a LSS, while coordinating a network of biological compartments with a variety of generation, consumption, and storage capabilities. A concentrated gas buffer tank is included in the system to demonstrate its capability to support the system operation flexibility and efficiency. Simulation analyses for changing O_2 demand scenarios are carried to assess the proposed control architecture performance.

1. Introduction

Life support systems (LSSs) are designed to provide the required environment for human beings to survive in outer space or isolated environments (Jones, 2003). The main objectives of LSSs are to regenerate the atmosphere, recycle water, supply the required amount of edible material to sustain human life, and process the waste generated in the system to provide maximum self-sustainability. LSSs were initially developed by space agencies to enable life in space due to their capability to self-regenerate residues using physicochemical technologies. Current LSSs are partially Earth-dependent as it happens in the International Space Station (ISS), with a scheduled re-supply of food and fresh water from Earth based on the crew needs. On average, an astronaut consumes 0.835, 3.909, and 0.617 kg per day of O_2, water, and food, respectively (Ehlmann et al., 2005). The journey to Mars, which is calculated to last up to 1100 days, makes it impossible to embark all crew needs due to the associated cargo load (Barta, 2017). Therefore, the future of space crewed missions, including the sustainable and long-term presence on Moon and Mars surfaces, will require the capability to sustain life autonomously (Gitelson and Lisovsky, 2002; Gòdia et al., 2004; Nelson et al., 2010; Schwartzkopf, 1992; Sulzman, 1994). LSSs can also provide advanced solutions for the severe challenges faced on Earth such as climate change and CO_2 accumulation, depletion of natural resources, clean water scarcity, or food crisis (Nelson et al., 2003). Controlled ecological LSSs (CELSSs) are LSSs driven by the use of artificial ecosystems based on advanced control strategies to guarantee its long-term operation and including the provision of food, which is not possible with purely physicochemical LSSs (Schwartzkopf, 1992). The most advanced human-made CELSS include ALSSTB (Texas, US), Biosphere-2 (Arizona, US), CEEF complex (Rokkasho, Japan), and MELiSSA (Micro-Ecological Life Support System Alternative (Gòdia et al., 2004)) with a pilot plant facility (MELiSSA Pilot Plant) implemented at Universitat Autonoma de Barcelona, Spain.

To have an operative CELSS, several complex subsystems need to be designed and integrated to achieve an operational loop satisfying many strict requirements. In this sense, a significant concern in integrating different biological subsystems is related to designing an efficient, reliable, and dynamic control system that can fulfill system requirements and guarantee its performance and long-term operation. Among the difficulties presented by this control problem, the different time constants of each compartment, the non-linearities found in the models, and especially the high degree of coupling between the variables to control are remarkable.

In 1991, Biosphere-2 experiments proved the importance and challenges of the controllability of CELSSs as microorganisms in the soil grew and released CO_2 into the atmosphere in an uncontrolled way, exceeding the capacity of plants to revitalize the

* Corresponding author.
E-mail address: Carles.Ciurans@uab.cat (C. Ciurans).

https://doi.org/10.1016/j.compchemeng.2021.107625

Nomenclature

Indexes

d	Phase: gas (g) or liquid (l)
x	Strain (i.e. L. indica, N. winogradskyi, N. europaea)
y	Compound index (i.e. O_2, CO_2)
z	Compartment index (C3, C4a, C5, membrane separation, concentrated gas tank, diluted gas tank)
n	C3 vol section nϵ{1..5}
i, j, m	Current sampling point at different control levels (3,2,1)
nom	Nominal point
ref	Reference
p	Sensor measurement. Ex. $C_y^z\|_d^p$ represents the measured value of $C_y^z\|_d$

Concentrated Gas Tank Parameters

$S^{CT,\ ref}$	Normalized reference level of the concentrated gas tank
$S^{CT,max}$/ $S^{CT,min}$	Normalized max/min level of the concentrated gas tank
S^{CT}	Normalized level of the concentrated gas tank
$P^{CT,\ max}$	Total maximum pressure of concentrated gas tank [Pa]
P^{CT}	Total pressure of concentrated gas tank [Pa]
$G^{CT/DT}$	Concentrated/Diluted gas tank discharging(+)/charging(-) rate [L h^{-1}]
$G^{CT,max}$/ $G^{CT,min}$	Maximum concentrated gas tank discharging/charging rate [L h^{-1}]
V^{CT}	Volume of the concentrated gas tank
N	Rate of moles [mole h^{-1}]
T	Temperature [K]
R	Gas constant [J K^{-1} mol^{-1}]

Internal Model Parameters

f_y	Dilution factor in the membrane separation for O_2, CO_2, and N_2 compounds

All Compartments

$\phi_y^z\|^I$	Rate of reaction of compound y in compartment z (subsection Iϵ{B_n} for C3) [g L^{-1} h^{-1}]
ϕ_x^z	Growth rate of strain x in compartment z [g L^{-1} h^{-1}]
$F_{in/out,I}^z$	Input/output liquid volumetric flow in compartment z. Subindex Iϵ{A, Bn, C, in, out, r} provides information about the flow localization within C3 reactor [L h^{-1}]
$G_{in/out,\ I}^z$	Input/output gas volumetric flow in compartment z. Subindex Iϵ{A, Bn, C, in, out, r} provides information about the flow localization within C3 reactor [L h^{-1}]
$M_y^z\|_d^{in/out}$	Input/Output mass flow of compoun(4d y in phase d in compartment z [g L^{-1} h^{-1}]. Extra superindex in can be included if referring to input mass flow.
Q_y^z	Production rate of compound y in compartment z [g h^{-1}]
$Q_y^{z,\ max/min}$	Max/min production rate of compound y in compartment z [g h^{-1}]
$C_y^z\|_d$	Concentration of compound y in phase d in compartment z [g L^{-1}]
$C_y^z\|_g^I$	Concentration of compound y in phase d in inflow/outflow of compartment z. x is used instead of y to refer to biomass. Superindex Iϵ{A, Bn, C, in, out, r} provides information about the localization within C3 reactor [g L^{-1}]
μ_x^z	Specific growth rate of strain x [h^{-1}] in compartment z
$\mu_x^{z,\ max}$	Maximum value of μ_x^z [h^{-1}]
$K_{x,g/m}^y$	Saturation constant of compound y for strain x. Subindex g/m refers to growth/maintenance [g L^{-1}]
d_x	Death rate of strain x [h^{-1}]
m_x	Maintenance rate of strain x [h^{-1}]
φ_y^z	Gas-Liquid transfer rate of compound y in compartment z [g L^{-1} h^{-1}]
K_La^z	Gas-liquid transfer coefficient (reactor design parameter) in compartment z [h^{-1}]
q_y	Partition coefficient of compound y
$C_y^z\|_d^*$	Saturation concentration of compound y in z (l indicates liquid phase) [g L^{-1}]
$Y_{\frac{y}{x},\ g/m}$	Yield of compound y over x. A subindex g/m can be included referring to growth/maintenance
Ψ_y^z	Limiting factor associated to substrate y at compartment z

Compartment C3 Parameters

ε	Bead void volume
ε_L	Liquid fraction of bed
ε_G	Gas fraction of bed
$V_{A/Bn/C}$	Volume of fraction A/ B, section n/C [L]
f	Liquid fraction of flow F back-mixed
f'	Gas fraction of flow F back-mixed

Compartment C4a Parameters

R	Radius of the bioreactor [m]
W	Light intensity [W m^{-2}]
$W_{day/night}^{nom}$	Day/night nominal light intensity [W m^{-2}]
K_j	Saturation constant for light [W m^{-2}]
α, δ	Radiative properties accounting for the absorption and scattering cross section of the cells and the fraction of radiant backscattered energy

Compartment C5 parameters

$resp_y^{C5}$	Respiration rate of compound y in C5 [mole h^{-1}]

Controller parameters

ΔQ_{O2}^{C4a}	Span of the C4a production rate [g h^{-1}]
$\Delta C_{O_2}\|_g^z$	Span of O_2 concentration in gas phase in compartment z [%]
ΔG_{CT}	Span of the gas flow from CT [L min^{-1}]
ρ	Dispatch factor $G_{in}^{C4a}/G_{out}^{C5}$
ρ^{max}/ρ^{min}	Max/min dispatch factor
λ_i	The ith weighting factor
$D_{O_2}^z$	O_2 consumption rate of compartment z [g h^{-1}]
N_{Pi}/N_{Ci}	Prediction/Control horizon at the ith control level
$T_{m,PFCi}$	First order process time constant, ith control level PFC [h^{-1}]
$K_{m,PFCi}$	First order process gain, ith control level PFC
$T_{s,i}$	Sampling time at the ith control level [h]
$CLRT_{PFCi}$	Closed loop response time at the ith control level PFC
MV	Manipulating Variable

Acronyms

CELSSs	Controlled ecological LSSs
HCS	Hierarchical control structure
ISS	International Space Station

LSS	Life support systems
MELiSSA	Micro-Ecological Life Support System Alternative
MG	Microgrid
MPC	Model Predictive Control
MS	Membrane separation
PFC	Predictive functional controller
VR-MPC	Varying-resolution MPC
PQ	Photosynthetic quotient

air while making the atmosphere unbreathable for the inhabitants (Nelson et al., 2003). In one of the longest runs of a CELSS test promoted by NASA in 1998, which included air revitalization coupled to food supply from crop culture and waste processing, the need for an integrated control system appeared to be essential to reduce crew and ground personnel intervention time (Nelson et al., 1993). A recent integration attempt in the MELiSSA Pilot Plant succeeded to provide revitalized air to the crew compartment solely from a photosynthetic compartment under the control of a Master-slave predictive functional controller (PFC) in operation during 50 days (Alemany et al., 2019). This represents an inspiring basis to design an advanced control system to integrate other compartments in the loop while supporting its performance.

Current LSS strategies in ISS does not include the production of edible material, but only the environmental control based on the O_2 generation and CO_2 removal. However, to improve the recycling capacity extending it to all metabolic wastes generated by the crew, it is mandatory to produce edible material that makes the use of photosynthetic compartments essential. This is the strategy followed by CELSS, which integrates photosynthetic compartments providing high levels of recycling and autonomy. In CELSS, sunlight represents the only fully available external resource, but in terms of mass exchange, a full closeness is expected.

In a CELSS, the limited degree of freedom, reduced size of the physical system, presence of multiple producers and consumers, tight technical and operational restrictions, and different dynamics interacting within and between compartments result in a complex control problem. However, there are other existing complex systems such as microgrids (MGs) that share similarities with LSSs and can inspire their control design and resource allocation.

MGs are known as local aggregations of distributed energy resources, energy storage systems, and loads with the capability of operating in both grid-connected and standalone modes. MGs are responsible to locally solve energy balance problems by controlling a variety of distributed energy resources and storage systems characterizing different dynamical behavior. The main goal is to supply MGs consumers with sustainable, reliable, and cost-effective energy and ensure optimal resource utilization through solving multi-time scale multi-objective control tasks while considering a number of operational and technical constraints and uncertainty at both demand and supply sides.

The similarities between MGs and specially islanded MGs and CELSS are considerable, including the existence of multiple suppliers and consumers, the uncertainties in the consumption and production patterns, the need to control optimally the elements involved in the loop, the importance of storage management as well as the key role of sun-derived energy, among others. The accumulated experience and success of MGs management offers the possibility to apply their advanced control approaches in CELSSs operation as already explored in Ciurans et al. (2021). A comparison between the two systems is presented in Fig. 1. In this sense, this paper extends the hierarchical control (Vasquez et al., 2010) and energy management of MGs to CELSS using the MELiSSA Pilot Plant, as a case study (Gòdia et al., 2004). The study focuses on developing a hierarchical control structure (HCS) to control O_2 concentration in the crew compartment ensuring the survivability of the crew through coordinating the operation of different available resources. A concentrated gas tank is included in the system to demonstrate its capability to support the system's operation flexibility and efficiency.

It should be noted that power and thermal subsystems also play important roles in a CELSS to provide the required energy to support different equipment operations and to maintain the temperature and humidity of different compartments within the desired boundaries. However, this paper only focuses on the mass balance and O_2 control of the CELSS, and integrating energy and thermal subsystems will be a future study of the authors.

The rest of this paper is organized as follows: Section 2 is devoted to the introduction of the selected case study and mathematical representation of its different subsystems. The outline of the proposed HCS is presented in Section 3 while discussing different control levels and associated methodologies, objective functions, and constraints. Simulation results are presented and discussed in Section 4. Finally, concluding remarks are given in Section 5.

2. Mathematical representation of the Melissa loop

MELiSSA is a CELSS made of a network of five biological compartments with limited matter exchange with the outside environment (Fig. 1) including an anaerobic reactor that converts residual wastes into CO_2 and volatile fatty acids called C1; a photoheterotrophic compartment that converts the volatile fatty acids into CO_2 (C2); a nitrification reactor that consumes O_2 to convert ammonium and urea into nitrate (C3); a photobioreactor that uses cyanobacteria to convert CO_2 and inorganic nitrogen into edible material and O_2 (C4a); and a higher plant chamber that is used to grow crops converting inorganic nitrogen and CO_2 into edible material and O_2 (C4b). All these compartments need to be coordinated to guarantee a safe environment for the crew compartment (C5) through the supply of O_2, water, and nutrients, air revitalization, and waste processing. MELiSSA loop should also exploit the sunlight through the biosynthetic reactions, maximize reaction yields, minimize the overall hardware mass and the energy expenditure, and guarantee the crew safety among other life support requirements provided in the ALISSE criteria (Brunet et al., 2010). The part of the process that is studied in this paper is represented in Fig. 2, which reproduces the current integration phase of the MELiSSA Pilot Plant, comprising C3, C4a, and C5 along with two gas buffer tanks. C3 and C4a are connected through the liquid phase while C3, C4a, C5, and the gas storing tanks are connected through the gas phase.

As can be seen in Fig. 2, starting from C5, the gas outflow of this compartment (G_{out}^{C5}), containing gas compounds with specific concentrations is split into two flows going to C4a (G_{in}^{C4a}) and the membrane separation unit (G_{in}^{MS}) whose output is a concentrated (G^C) and a diluted (G^D) O_2 flow. A specific fraction of the concentrated gas flow is the input of C3 (G_{in}^{C3}) that is determined based on the amount of ammonia to be oxidized in the liquid inflow being fed to C3 (F_{in}^{C3}). The other fraction ($G^C - G_{in}^{C3}$) is sent back to C5 and can be used to fill the concentrated gas tank. The gas outflow of C3 (G_{out}^{C3}) and C4a (G_{out}^{C4a}) are sent back to C5 together with the gas flows coming from the membrane separation closing the gas loop as shown in the following equations.

$$G_{in}^{C5} = G_{out}^{C4a} + G_{out}^{C3} + G_{rich} + G^D + G^{DT} \tag{1}$$

$$G_{rich} = \left(G^C - G_{in}^{C3}\right) + G^{CT} \tag{2}$$

The gas buffer tanks are appropriately sized to satisfy the O_2 demand of one human for 24 h with a maximum pressure of

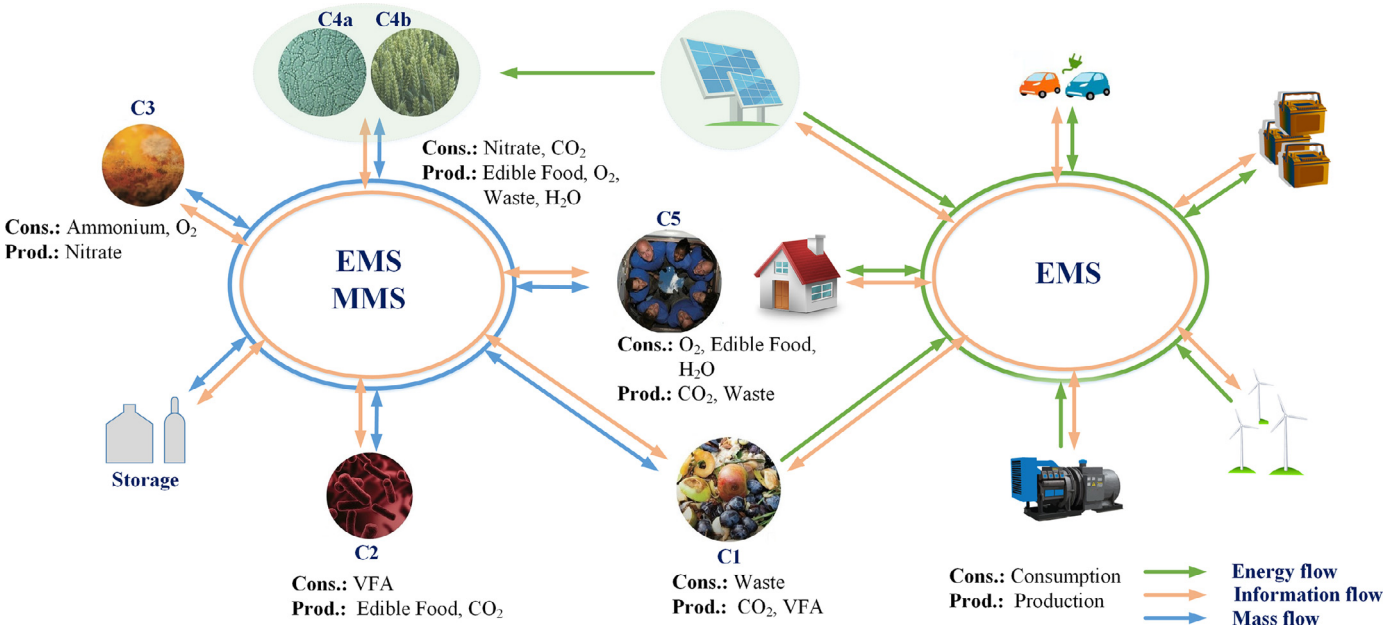

Fig. 1. An exemplary life support system (left) and a Microgrid (right).

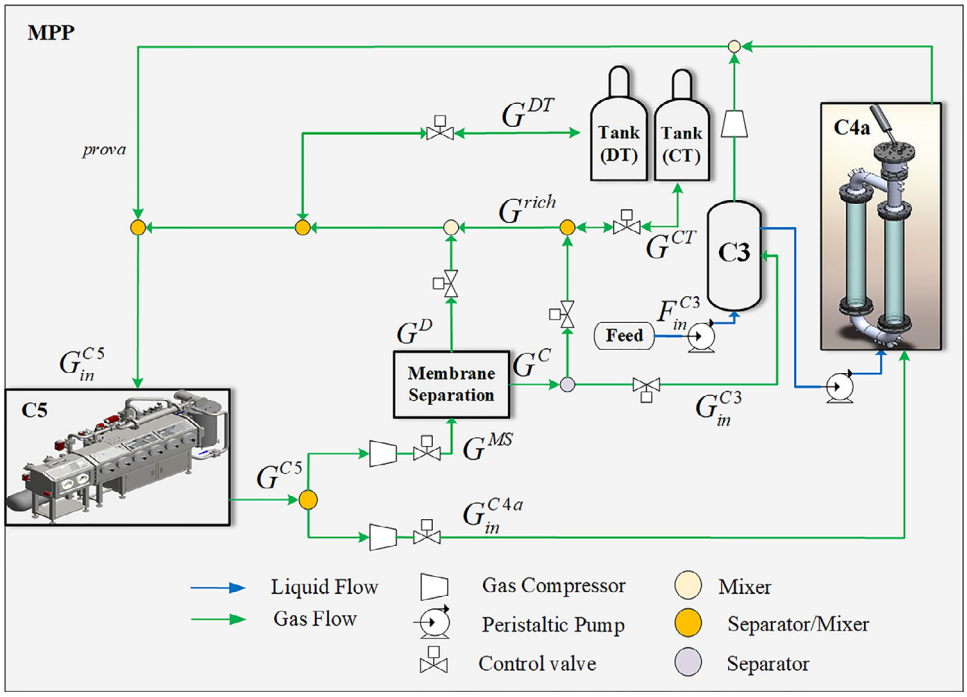

Fig. 2. The layout of the system under study.

50 bar and 10 L of volume. Considering that the MELiSSA Pilot Plant has not yet integrated the higher plant chamber (C4b), which represents the main producer of O_2, only 3 rats (out of the maximum capacity of C5 of 40 rats, approximately equivalent to one human in terms of physiological needs) are inhabiting C5, which have an O_2 consumption rate that can be supplied solely by C4a. Currently, the liquid phase loop is still not closed, but its closure is expected in the upcoming MELiSSA Pilot Plant activities.

Non-linear mechanistic models are available for each of these compartments validated with massive experimental data obtained in the MELiSSA Pilot Plant testing campaigns. C3 model was validated and calibrated in a 120-day standalone experiment using step changes of ammonium loads (0.3–0.6 g N–NH4/L) and residence times (5 – 80 h) (Pérez et al., 2005a), while C4a and C5 models were evaluated in two 50 and 30-day integration tests by applying step changes to O_2 setpoints (19–22%) of the crew compartment (Alemany et al., 2019). Interested readers are referred to (Cornet et al., 1995; Cruvellier et al., 2017; Dauchet et al., 2016; Poughon et al., 1999) for more information.

The process described in Fig. 2 operates in a continuous mode for both the liquid and gas phases. Thus, the law of conservation of mass needs to be satisfied in each of the biological compartments C3, C4a, and C5. Each compartment includes several compounds from a list of 23 compounds including H_2O, NH_3, H_2SO_4, H_3PO_4, HNO_3, HNO_2, Urea, O_2, CO_2, Acetic, Propionic, Butyric, Valeric and Caproic Acid, N_2, H_2, CH_4, Inert gases, Organic Matter, *Ni-*

trosomonas, Nitrobacter, Rhodobacter, and *Limnospira* Biomass. Accordingly, instead of introducing the dynamical equations of individual compounds of each compartment, the general governing equations of each compartment will be introduced.

A bioreactor working in continuous mode with a biochemical transformation of compound y can be defined with the following generic form:

$$\dot{C}_y^z|_d = M_y^z|_d^{in} - M_y^z|_d^{out} + \phi_y^z + \varphi_y^z \tag{3}$$

$$\phi_x^z = \mu_x^z \cdot C_x^z|_l \tag{4}$$

$$\mu_x^z = \mu_x^{z,\ max} \cdot \Psi_y^z - d_x \tag{5}$$

$$\Psi_y^z = \frac{C_y^z|_l}{C_y^z|_l + K_{x,g}^y} \tag{6}$$

$$\phi_y^z = \phi_x^z \cdot Y_{\frac{y}{x}} \tag{7}$$

Notice in (4)-(7), rate of reaction (ϕ_y^z) only affects the liquid phase, being the rate of reaction zero in the gas phase. According to (3), the changes in the concentration of the y^{th} compound ($\dot{C}_y^z|_d$) in compartment z in phase d (gas/liquid) is specified by the mass inflow ($M_y^z|_d^{in}$) and outflow ($M_y^z|_d^{out}$), the rate of reaction (ϕ_y^z) and the phase exchange rate (φ_y^z) in the associated compartment. In case of multiple substrates, (6) is modified to include the product of all participating substrates and Ψ_Π^z is defined for N_y compounds as follows:

$$\Psi_\Pi^z = \prod_{y=1}^{N_y} \frac{C_y^z|_l}{C_y^z|_l + K_{x,g}^y} \tag{8}$$

To obtain the production and consumption rates including maintenance costs, expression (7) becomes:

$$\phi_y^z = \left(\frac{\mu_x^{z,max} \cdot C_y^z|_l}{C_y^z|_l + K_{x,g}^y} \cdot Y_{\frac{y}{x},g} + \frac{m_x \cdot C_y^z|_l}{C_y^z|_l + K_{x,m}^y} \cdot Y_{\frac{y}{x},m} \right) \cdot C_x^z|_l \tag{9}$$

The gas-liquid transfer rate defined by φ_y^z takes the following form:

$$\varphi_y^z = K_L a^z \cdot \left(C_y^z|_l{}^* - C_y^z|_l \right) \tag{10}$$

$$C_y^z|_l{}^* = \frac{C_y^z|_l}{q_y} \tag{11}$$

Notice that considering the continuous mode of operation of the compartments and assuming that the biochemical transformation that takes place does not imply density changes in either of the liquid or gas phases, the volumetric input and output flow is maintained, i.e. $G_{in}^z = G_{out}^z$ and $F_{in}^z = F_{out}^z$.

2.1. C3 Compartment model

The design of C3 is based on a packed-bed reactor with immobilized cells that carry the oxidation of ammonia to nitrate by ammonia-oxidizing *Nitrosomonas europaea* and nitrite-oxidizing *Nitrobacter winogradskyi*. To capture properly the C3 dynamics, the total module is discretized in seven volumes as shown in Fig. 3. In this figure, V_A and V_C are the volumes at the top and bottom of the reactor, which are used for probe location, gas, and liquid inlet, recirculation and outlet flows, but where no reaction takes place. V_B includes the packed-bed part of the bioreactor where cells are immobilized and the reaction takes place. V_B is discretized in five parts to cope with the hydrodynamics and to account for non-ideal liquid mixing for implementing the reaction kinetics.

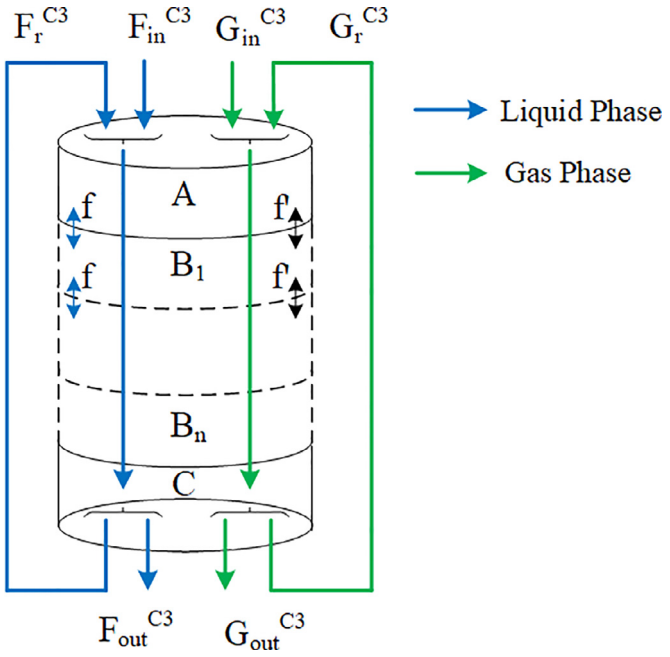

Fig. 3. Illustration of the design of Compartment 3.

The dynamical evolutions of parts A, B, and C of the compartment in both liquid and gas phases are derived by the following general equations where $F_{int}^{C3}/G_{int}^{C3}$ is the sum of liquid/gas inflow to C3 (F_{in}^{C3}/G_{in}^{C3}) and recirculation liquid/gas flux (F_r^{C3}/G_r^{C3}) (Pérez et al., 2005b; Poughon et al., 1999):

Part A

$$\begin{aligned} V_A \cdot (1-\varepsilon_G) \cdot \dot{C}_y^{C3}|_l^A &= F_{in}^{C3} \cdot C_y^{C3}|_l^{in} + F_r^{C3} \cdot C_y^{C3}|_l^r \\ &- F_{int}^{C3} \cdot \left((f+1) \cdot C_y^{C3}|_l^A - f \cdot C_y^{C3}|_l^{B1} \right) \\ &+ V_A \cdot (1-\varepsilon_G) \cdot \varphi_y^{C3} \end{aligned} \tag{12}$$

$$\begin{aligned} V_A \cdot (1-\varepsilon_L) \cdot \dot{C}_y^{C3}|_g^A &= G_{in}^{C3} \cdot C_y^{C3}|_g^{in} + G_r^{C3} \cdot C_y^{C3}|_g^r \\ &- G_{int}^{C3} \cdot \left((f'+1) \cdot C_y^{C3}|_g^A - f' \cdot C_y^{C3}|_g^{B1} \right) \\ &- V_A \cdot (1-\varepsilon_L) \cdot \varphi_y^{C3} \end{aligned} \tag{13}$$

Part B

$$\begin{aligned} V_{Bn} \cdot \varepsilon \cdot (1-\varepsilon_G) \cdot \dot{C}_y^{C3}|_l^{Bn} &= F_{int}^{C3} \cdot \left((f+1) \cdot C_y^{C3}|_l^{Bn-1} \right. \\ &+ f \cdot C_y^{C3}|_l^{Bn+1} - \left((f+1) \cdot C_y^{C3}|_l^{Bn} + f \cdot C_y^{C3}|_l^{Bn} \right) \Big) \\ &+ V_{Bn} \cdot \varepsilon \cdot (1-\varepsilon_G) \cdot \left(\phi_y^{C3}|^{Bn} + \varphi_y^{C3} \right) \end{aligned} \tag{14}$$

$$\begin{aligned} V_{Bn} \cdot \varepsilon \cdot (1-\varepsilon_L) \cdot \dot{C}_y^{C3}|_g^{Bn} &= G_{int}^{C3} \cdot \left((f'+1) \cdot C_y^{C3}|_g^{Bn-1} + f' \cdot C_y^{C3}|_g^{Bn+1} \right. \\ &- \left((f'+1) \cdot C_y^{C3}|_g^{Bn} + f' \cdot C_y^{C3}|_g^{Bn} \right) \Big) \\ &- V_{Bn} \cdot \varepsilon \cdot (1-\varepsilon_L) \cdot \varphi_y^{C3} \end{aligned} \tag{15}$$

Part C

$$\begin{aligned} V_C \cdot (1-\varepsilon_G) \cdot \dot{C}_y^{C3}|_l^C &= F_{int}^{C3} \cdot \left((f+1) \cdot C_y^{C3}|_l^{B_5} - f \cdot C_y^{C3}|_l^C \right) \\ &- F_r^{C3} \cdot C_y^{C3}|_l^C - F_{out}^{C3} \cdot C_y^{C3}|_l^C \\ &+ V_C \cdot (1-\varepsilon_G) \cdot \varphi_y^{C3} \end{aligned} \tag{16}$$

$$\begin{aligned} V_C \cdot (1-\varepsilon_L) \cdot \dot{C}_y^{C3}|_g^C &= G_{int}^{C3} \cdot \left((f'+1) \cdot C_y^{C3}|_g^{B_5} - f' \cdot C_y^{C3}|_g^C \right) \\ &- F_r^{C3} \cdot C_y^{C3}|_g^C - G_{out}^{C3} \cdot C_y^{C3}|_g^C \\ &- V_C \cdot (1-\varepsilon_L) \cdot \varphi_y^{C3} \end{aligned} \tag{17}$$

2.2. C4a Compartment model

The hydrodynamic pattern of C4a is approximated to a perfectly mixed photobioreactor, which is responsible for the conversion of CO_2 from C5 and nitrate from C3 into O_2 and biomass for human consumption while the reaction is controlled by light when no substrate is limiting. The reaction is carried by the cyanobacteria *Limnospira indica*. The general mass balance equation for this bioreactor is given in (3). The growth rate term in C4a is slightly different from (4) as light energy transfer is considered a rate-limiting process (Cornet et al., 1992). The following equation is used to calculate the growth rate of L. *indica* and consumption or production rates of compound y:

$$\phi_x^{C4a} = \mu_x^{C4a,\ max} \cdot \Psi_{\Pi}^{C4a} \cdot \frac{1}{\pi \cdot R^2} \int_{Ril}^{R} 2\pi r \frac{4\pi J_r}{K_j + 4\pi J_r} dr \tag{18}$$

$$\phi_y^{C4a} = \phi_x^{C4a} \cdot Y_{\frac{y}{x},\ g} \tag{19}$$

In (18), *Ril* is the illuminated radius defined as the photobioreactor radius where light reaches the compensation point. In addition, J_r represents the profile of the light radiant energy and it is expressed as a quotient of the modified Bessel functions of the first kind as follows:

$$J_r = \frac{W \cdot I_0(\delta \cdot r)}{I_0(\delta \cdot L) + \alpha \cdot I_1(\delta \cdot L)} \tag{20}$$

In (20), α and δ characterize the radiative properties of L. *indica*. The term Ψ_{Π}^{C4a} introduced in (8) considers the use of H_2NO_3, H_3PO_4, and CO_2 as substrates (Alemany et al., 2019).

2.3. C5 Compartment model

The dynamical model of compartment C5 takes into account the respiration dynamics of the crew ($resp_y^{C5}$), which, as mentioned above, is simulated by a group of three rats. It should be mentioned that no liquid phase in C5 is considered in the simulation presented in this study. The general equation for the respiration dynamics in C5 is represented below.

$$\dot{C}_y^{C5}|_g = G_{in}^{C5} \cdot C_y^{C5}|_g^{in} - G_{out}^{C5} \cdot C_y^{C5}|_g + resp_y^{C5} \tag{21}$$

In (21), $resp_y^{C5}$ is assumed to take two values for day and night shifts for O_2 and CO_2. In addition, G_{in}^{C5} is the inflow of C5 coming from other compartments as represented in (1), while G_{out}^{C5} is the compartment outflow that is split between C4a and the membrane separator as shown in Fig. 2 (Alemany et al., 2019).

2.4. Membrane Separation

In the membrane module, compounds are distributed in a concentrated (G^C) and a diluted (G^D) flow, being the latter higher than the first, with a concentration of $C_y^C|_g$ and $C_y^D|_g$ respectively:

$$C_y^D|_g = \frac{f_y \cdot G^{MS} \cdot C_y^{MS}|_g}{G^D} \tag{22}$$

$$G^D = \sum_{y \in \{O_2, CO_2, N_2\}} f_y \cdot G^{MS} \cdot C_y^{MS}|_g \tag{23}$$

$$C_y^C|_g = \frac{G^{MS} \cdot \left(C_y^{MS}|_g - f_y \cdot G^{MS} \cdot C_y^{MS}|_g\right)}{G^C} \tag{24}$$

$$G^C = \sum_{y \in \{O_2, CO_2, N_2\}} G^{MS} \cdot C_y^{MS}|_g - \left(f_y \cdot G^{MS} \cdot C_y^{MS}|_g\right) \tag{25}$$

2.5. Storage Gas tanks

The concentrated gas tank can be charged or discharged according to the O_2 needs of the overall system. The mission of the concentrated gas tank is to store concentrated O_2 to support C4a for supplying O_2 to the system. The ideal gas law is supposed to apply for the gas in the tank to calculate the rate of moles *(N)* introduced or removed during charging and discharging periods as shown below:

$$N = \frac{P^{CT} \cdot G^{CT}}{R \cdot T} \tag{26}$$

The normalized state of storage of the gas tank is calculated as follows:

$$S^{CT} = \frac{P^{CT}}{P^{CT,max}} \tag{27}$$

To maintain the mass flow in the loop, a diluted gas tank is included in the model as can be seen in Fig. 2, whose function is to release gas when the concentrated gas tank is filled and to be filled when the concentrated gas tank is emptied.

3. Method: HCS of the Melissa pilot plant

In this Section, the hierarchical control and energy management strategies of MGs are extended to CELSS. In general, MGs control is organized in a hierarchical structure including three control levels, namely primary, secondary, and tertiary. The primary control level is responsible for voltage/frequency regulation and power sharing among distributed resources and features the fastest control response. The secondary controller is responsible for restoring voltage/frequency to their nominal values while maintaining them in the permissible boundaries. Finally, the tertiary control level at the top of the hierarchy and with the largest time scale is responsible for optimal system operation and guaranteeing long-term efficient, economic, and resilient operation of the system.

Similarly, in a CELSS, to accommodate different time scales of the various processes in the loop and considering the complexity of the integrated control problem, different control tasks including mass flow regulation, flow dispatch, and optimal resource utilization can be distributed in different control levels. Accordingly, the proposed control structure is organized into three levels. Since each level of control follows different operating goals and responds to different dynamics, different frequencies (clock signals in Fig. 4) are used for updating the control commands. While Level 3 aims at deriving long-term control commands for O_2 supply from C4a and the concentrated gas tank, the lower-level controllers are responsible for determining short-term detailed control signals ensuring gas balance, and satisfying the system safety requirements. In Fig. 4, a general overview of the proposed control architecture is presented. A detailed description of each control level will be given in the following parts.

The main challenge is to design a control architecture that can manage the integrated operation of multiple producers and consumers of O_2. The most important priority of the process under study is to maintain the O_2 level in the crew compartment at a target level of around 21% at one bar of total pressure without violating the critical boundaries for CO_2. The definition of the upper boundary for carbon dioxide concentration in the crew compartment has been based on the maximum CO_2 concentration of 3% achieved in the MELiSSA Pilot Plant. This is acceptable for a test-bed hosting rats, as mock-up crew, whose environment control is ruled by the directive 2010/63/EU which suggests minimizing toxic pollutants (European Comission, 2010). For future human-based habitats, the environment control will be subject to the concentration range of 0.3–0.7% CO_2 defined by the NASA standard [V2–6004], which has become more restricted through the years

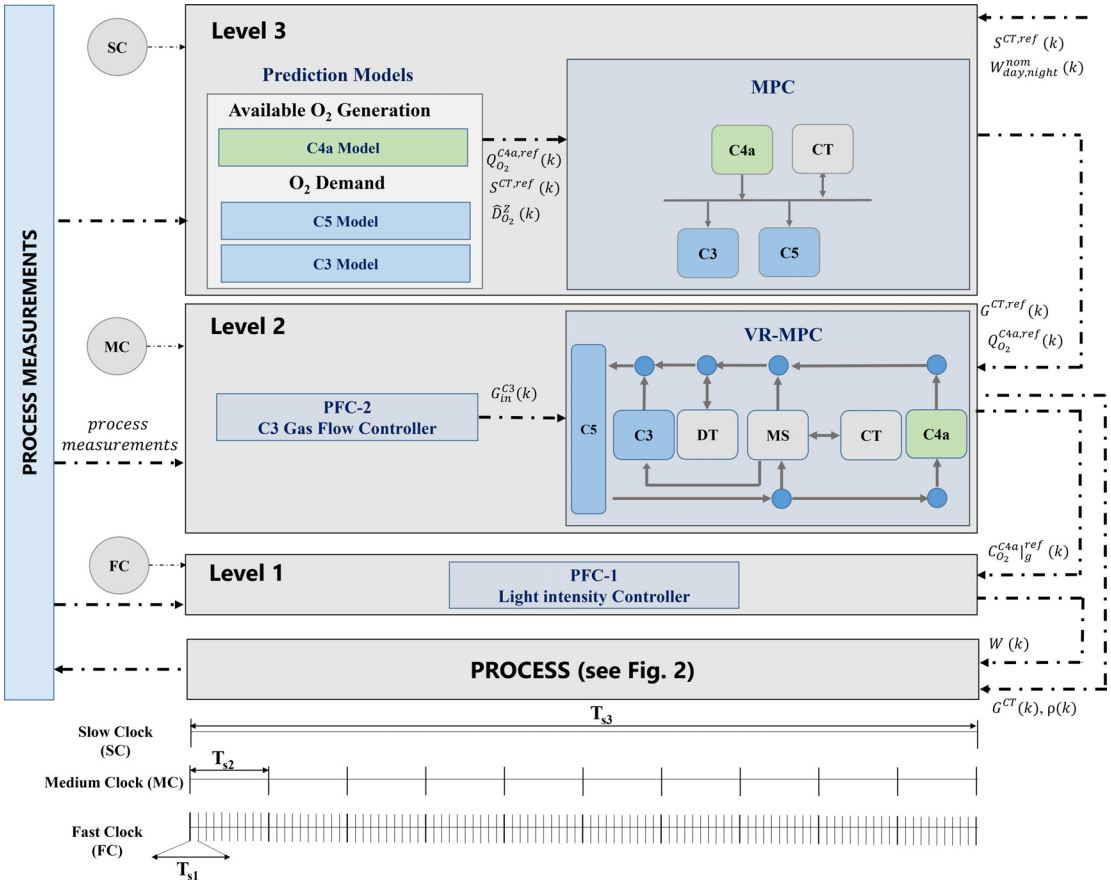

Fig. 4. The proposed hierarchical control structure.

according to the evidence from operational and research data. This can be easily achieved through the inclusion of a higher plants compartment, which have a notably lower photosynthetic quotient (PQ) for most of the crops under consideration for Life Support Systems compared to the PQ of L. *indica* used in C4a, driving the reduction of the overall carbon concentration in the system. This is included in the next MELiSSA Pilot Plant integration steps, but not in this study. Regarding oxygen control, NASA standard [V2–6003] requires a mild hypoxia limit of 16% (NASA, 2019) with the reference established at 21%.

To achieve these requirements, besides tuning and properly scaling the process design, appropriate control methods are necessary at each control level considering the control performance such as control functionality or controller response time, among others. In this regard, model predictive control (MPC) is adopted at Levels 2 and 3 of the proposed structure taking into account its capability to consider for the future predicted behavior of the system, system constraints, its capacity to deal with non-linear multiple-input multiple-output processes (Michael A.Henson, 1998) and to express the desired performance specifications through adjusting control objectives (Ocampo-Martinez et al., 2012). Predictive functional control (PFC) is also used at Levels 1 and 2 because of its simplicity, low computational time requirement, and ease of implementation (Richalet, 1993).

PFC is a simplified variant of MPC that is characterized by replacing the control and prediction horizon of MPC with a coincidence point. When only one coincidence point is used, instead of minimizing the difference between the predicted output of the system and the desired trajectory over the desired horizon, the goal is to match the model output and the target trajectory at the coincidence point by solving a simple algebraic equation. In this paper, PFC is applied to a simplified first-order approximation of subsystems assuming one coincidence point.

Considering a first-order difference equation for a given compound $C^z_y|_d$ and a manipulated variable (MV):

$$C^z_y|_d(k+1) = \alpha_{m,PFC} \cdot C^z_y|_d(k) + K_{m,PFC} \cdot \beta_{m,PFC} \cdot MV(k) \tag{28}$$

$$\alpha_{m,PFC} = e^{-Ts/T_{m,PFC}} \tag{29}$$

$$\beta_{m,PFC} = 1 - \alpha_{m,PFC} \tag{30}$$

The reference trajectory ($C^z_y|^{ref}_d$) is considered to be of the first-order type whose starting point is equal to the value of the measured process output ($C^z_y|^{p}_d$) at the current time step. Assuming the coincidence point equal to one, the predicted value of the process output one step later than the present can be calculated as follows:

$$\Delta\hat{C}^z_y|_d(k+1) = \left[C^z_y|^{ref}_d(k) - C^z_y|^{p}_d(k)\right] \cdot \left[1 - e^{\left(\frac{-3 \cdot Ts}{CLRT_{PFC}}\right)}\right] \tag{31}$$

The parameter CLRT can be used to adjust the speed of response. After some algebraic operations using (28)-(31), it is straightforward to obtain the following control law:

$$MV(k) = \frac{\left[C^z_y|^{ref}_d(k) - C^z_y|^{p}_d(k)\right] \cdot lh_{PFC} + \beta_{m,PFC} \cdot \hat{C}^z_y|_d(k)}{K_{m,PFC} \cdot \beta_{m,PFC}} \tag{32}$$

$$lh = 1 - \left(e^{-3 \cdot Ts/CLRT_{PFC}}\right) \tag{33}$$

In the proposed control structure, PFC is used at Level 2 to adjust the input gas flow of C3 (G^{C3}_{in}) according to the amount of ammonium introduced in C3 that needs to be oxidized to nitrate. PFC is also used at Level 1 to adjust the light energy input in C4a.

Other primary and device-level controllers are also mostly based on PFC controllers. In the following, the control strategies at different control levels along with the associated control objectives and constraints are presented.

3.1. Level 3: Tertiary controller

This is the system-level controller responsible for designing optimal long-term operating setpoints for the local controllers while optimizing the use of resources and satisfying different technical and operational constraints. To do so, a prediction is made based on the optimal operating criteria prescribed by the supervisory controller. These operating criteria include keeping the level of the concentrated gas tank around a reference level ($S^{CT,\ ref}$) of 50% over the total volume of 10 L and a maximum pressure of 50 bar and to operate C4a around two nominal light levels for day and night shifts ($W^{nom}_{day/night}$). To draw the prediction, measurements are obtained from the monitoring system and used to initialize the internal model described in Section 2. On the one hand, the upper bound of the O_2 production rate of C4a ($Q^{C4a,\ max}_{O2}$) is set by running the internal model using the maximum light intensity technically allowed while its reference production rate ($Q^{C4a,ref}_{O2}$) is determined using the nominal light intensity. On the other hand, O_2 consumption rates by C3 and C5 ($\hat{D}^{C3}_{O_2}$ and $\hat{D}^{C5}_{O_2}$ respectively) are predicted over the Level 3 prediction horizon. Hence, references regarding the predicted O_2 consumption and production rates are generated and used to solve the following optimization problem:

$$J_T = \min_U \lambda_1 J_1 + \lambda_2 J_2 \tag{34}$$

$$J_1 = \sum_{k=1}^{Np_1} \left(\hat{S}^{CT}(i+k|i) - S^{CT,ref}\right)^2 \tag{35}$$

$$J_2 = \sum_{k=0}^{Nc_1-1} \left(\frac{Q^{C4a}_{O2}(i+k|i) - \hat{Q}^{C4a,ref}_{O2}(i+k|i)}{\Delta \hat{Q}^{C4a}_{O2}(k)} \right)^2 \tag{36}$$

$$U = \begin{bmatrix} Q^{C4a}_{O2}(i) \\ G^{CT}(i) \\ \vdots \\ Q^{C4a}_{O2}(i+Np_1-1) \\ G^{CT}(i+Np_1-1) \end{bmatrix} \tag{37}$$

$$U_3 = \begin{bmatrix} Q^{C4a}_{O2}(i) & G_{CT}(i) \end{bmatrix} \tag{38}$$

Subject to:
(26)-(27)

$$\sum_{z\in\{C3,C5\}} \hat{D}^{z}_{O_2}(i+k|i) = Q^{4a}_{O_2}(i+k|i) + \hat{Q}^{CT}_{O_2}(i+k|i) \tag{39}$$

$$G^{CT,min} \le G^{CT}(i+k|i) \le G^{CT,max} \tag{40}$$

$$Q^{C4a,\ min}_{O2}(i+k|i) \le Q^{4a}_{O_2}(i+k|i) \le \hat{Q}^{C4a,\ max}_{O2}(i+k|i) \tag{41}$$

$$S^{CT,min} \le \hat{S}^{CT}(i+k|i) \le S^{CT,max} \tag{42}$$

In (39)-(42), k $\in$ {0,...,Np_1−1}. $\hat{S}^{CT}(i+k|i)$, $\hat{D}_{O_2}(i+k|i)$, $\hat{Q}^{C4a,max}_{O2}(i+k|i)$ and $\hat{Q}^{CT}_{O_2}(i+k|i)$ denote the predicted concentrated gas tank storage level, the total O_2 demand ($\hat{D}^{C3}_{O_2} + \hat{D}^{C5}_{O_2}$), the C4a maximum production rate and the concentrated gas tank production or consumption rate respectively at time step $i+k$ using the internal model with the information available at time step i. The constraint represented in (39) indicates that the consumption rate expected for the compartments C3 and C5 must be satisfied with the production from C4a and the concentrated gas tank. The outputs of the tertiary controller stored in U_3 are considered as the reference for the secondary controller (see Fig. 4). In (35), $S^{CT,ref}$ represents the reference value for the state of the storage in the tank, which in this study is assumed to be fixed and time-invariant. In our future work, the operating criteria are expected to be dynamically adapted by the supervisory controller using a techno-economical and reliability analysis following the LSSs requirements such as the ALISSE criteria. Range parameters are included in the objective functions for normalization purposes due to the different magnitude of process variables.

3.2. Level 2: Secondary controller

The main functionality of the secondary controller is to keep the gas concentration of the crew compartment within a safe boundary by manipulating the gas flows and the O_2 concentration in C4a. The output of this level of control is provided to local controllers as the reference trajectory for the following time intervals. The secondary controller needs to follow the outcome of the tertiary controller as it accounts for the optimal resource distribution and is based on the long-term prediction of the process. The sample time of this level is shorter than that of Level 3, in line with its scope to correct O_2 concentration deviations in C5. Two interrelated controllers work at the secondary level: (1) a PFC-based controller (PFC 2) that determines the flow of gas (G^{C3}_{in}) required to oxidize the nitrogen demands according to the ammonia concentration fed to C3 in the liquid phase (F^{C3}_{in}, see Fig.2), and (2) a non-linear varying-resolution MPC (VR-MPC) controller that generates the reference values for gas flows and the O_2 concentration in C4a to be followed by the local controllers (see Fig. 4). To do so, the VR-MPC requires the information from PFC-2.

3.2.1. Predictive functional control

At the secondary level, a PFC-based control strategy is used to adjust the flow of enriched O_2 gas to convert ammonium into nitrate. The internal model used is based on a first-order approximation of O_2 concentration of C3 in the liquid phase ($C^{C3}_y|_l$) with the input gas flow (G^{C3}_{in}) as the manipulated variable. The first order process gain and time constant have been identified in Alemany et al. (2019) based on several experimental tests conducted in the pilot plant. Further details regarding the identification and validation of the first-order models for C3 and C4a controllers can be found in Alemany et al. (2019). It is worth mentioning that these parameters are assumed to be fixed in this paper. However, as the system operating condition and the plant environment are exposed to changes over time, these parameters need to be re-tuned. Two different strategies can be followed for re-tuning of the model parameters, a regular time-based re-tuning strategy or an event-based technique continuously monitoring a performance index to trigger the re-tuning process. In the former strategy, a fixed frequency is determined based on the historical data and experts' knowledge to re-tune the model parameters while in the latter, a performance index is defined for the model. Monitoring the performance index and comparing it with the desired threshold reflecting the permissible level of performance degradation, the time for triggering the re-tuning process is determined. Using the first-order model parameters given in Alemany et al. (2019) and (28)-(33), the following control law can be obtained:

$$G^{C3}_{in}(j) = \frac{\left[C^{C3}_{O_2}|^{ref}_l(j) - C^{C3}_{O_2}|^{p}_l(j)\right] \cdot lh_{PFC2} + \beta_{m,PFC2} \cdot \hat{C}^{C3}_{O_2}|_l(j)}{K_{m,PFC2} \cdot \beta_{m,PFC2}} \tag{43}$$

$$G^{C3}_{in}(j) \ge 0 \tag{44}$$

In (43), $C_{O_2}^{C3}|_l^{ref}$ is the reference of the O_2 concentration of C3 in the liquid phase, which is obtained from the O_2 demand predicted by the prediction system at the tertiary level. Hence, at the current time step of the tertiary and the secondary controllers:

$$C_{O_2}^{C3}|_l^{ref}(j) = \frac{\hat{D}_{O_2}^{C3}}{V_{C3} \cdot K_L a^{C3}} \tag{45}$$

3.2.2. Varying-Resolution MPC

The output of this controller includes the gas flows to C4a (G_{in}^{C4a}) and to the membrane separation unit (G_{in}^{MS}), the gas flow to add or retrieve from the concentrated gas tank (G^{CT}) and the diluted gas tank (G^{DT}) and the O_2 concentration in the outflow of C4a ($C_{O_2}^{C4a}|_g$). The prediction and control horizons are set to one hour and the sample time is set to 6 min. However, using a 6-min time resolution over the entire horizon of 1-hour results in a 10-step problem, which cannot be efficiently solved in a reasonable time. Hence, a homogeneous time resolution is not appropriate over the 1-hour time span. While in the first next steps, a higher resolution is preferred due to more accurate information, in the later steps, with fewer certain scenarios, the resolution can be decreased (Olivares et al., 2014). Accordingly, five time steps with different time resolutions are considered: 2 × 6-min, 2 × 12-min, and 1 × 24-min time-steps. The multi-objective control problem at the secondary level is summarized below where λ_i represent weighting coefficients:

$$J_S = \min_Y (\lambda_3 J_3 + \lambda_4 J_4 + \lambda_5 J_5 + \lambda_6 J_6 + \lambda_7 J_7) \tag{46}$$

$$J_3 = \sum_{k=1}^{Np_2} \left(\frac{\hat{C}_{O_2}^{C5}|_g(j+k|j) - C_{O_2}^{C5}|_g^{ref}}{\Delta C_{O_2}^{C5}|_g} \right)^2 \tag{47}$$

$$J_4 = \sum_{k=0}^{Nc_2-1} \left(\frac{G^{CT}(j+k|j) - G^{CT,ref}(j+k|j)}{\Delta G^{CT}} \right)^2 \tag{48}$$

$$J_5 = \sum_{k=0}^{Nc_2-1} \left(\frac{\hat{Q}_{O2}^{C4a}(j+k|j) - Q_{O2}^{C4a,ref}(j+k|j)}{\Delta \hat{Q}_{O2}^{C4a}(j+k|j)} \right)^2 \tag{49}$$

$$J_6 = \sum_{k=0}^{Nc_2-1} (\rho(j+k|j) - \rho(j+k-1|j))^2 \tag{50}$$

$$J_7 = \sum_{k=0}^{Nc_2-1} \left(\frac{\hat{C}_{O_2}^{C4a}|_g(j+k|j) - \hat{C}_{O_2}^{C4a}|_g(j+k-1|j)}{\Delta C_{O_2}^{C4a}|_g} \right)^2 \tag{51}$$

$$Y = \begin{bmatrix} y_1 \\ \vdots \\ y_{Np_2-1} \end{bmatrix} \tag{52}$$

$$y_1 = \begin{bmatrix} \rho(j) \\ G^{CT}(j) \\ C_{O_2}^{C4a}|_g(j) \end{bmatrix}; y_{Np_2-1} = \begin{bmatrix} \rho(j+Np_2-1) \\ G^{CT}(j+Np_2-1) \\ C_{O_2}^{C4a}|_g(j+Np_2-1) \end{bmatrix} \tag{53}$$

$$U_2 = \begin{bmatrix} \rho(j) & G_{CT}(j) & C_{O_2}^{C4a}|_g(j) \end{bmatrix} \tag{54}$$

Subject to:

$$\textit{System dynamics } (21) - (27) \tag{55}$$

$$G_{out}^{C5}(j+k-1|j) = G_{in}^{C4a}(j+k|j) + G_{in}^{MS}(j+k|j) \tag{56}$$

$$\rho(j+k|j) = \frac{G_{in}^{C4a}(j+k|j)}{G_{out}^{C5}(j+k|j)} \tag{57}$$

$$G^{CT,min} \le G^{CT}(j+k|j) \le G^{CT,max} \tag{58}$$

$$S^{CT,min} \le \hat{S}_{CT}(j+k|j) \le S^{CT,max} \tag{59}$$

$$C_{O_2}^{C5}|_g^{min} \le \hat{C}_{O_2}^{C5}|_g(j+k|j) \le C_{O_2}^{C5}|_g^{max} \tag{60}$$

$$C_{CO_2}^{C5}|_g^{min} \le \hat{C}_{CO_2}^{C5}|_g(j+k|j) \le C_{CO_2}^{C5}|_g^{max} \tag{61}$$

$$C_{O_2}^{C4a}|_g^{min} \le C_{O_2}^{C4a}|_g(j+k|j) \le C_{O_2}^{C4a}|_g^{max} \tag{62}$$

$$\rho^{min} \le \rho(j+k|j) \le \rho^{max} \tag{63}$$

The cost function (46) is the weighted sum of the normalized cost functions associated with the deviation of O_2 concentration in C5 from the reference as represented in (47), the deviation of the O_2 provided by the concentrated gas tank and C4a from the references scheduled at the tertiary level represented in (48) and (49) and the rate of change of manipulated variables represented in (50)-(51).

It is worth mentioning that due to the restricted computation time of the secondary controller, the dynamic equations corresponding to the evolution of O_2 and CO_2 in C3 and C5 have been reduced to fixed consumption rates. In addition, an empirical approximation has been used to estimate CO_2 concentration in C4a given the decision variable $C_{O_2}^{C4a}|_g$. Hence, all the models are discretized to be used in the above-mentioned MPC framework. The outputs of the secondary controller stored in U_2, together with the output of PFC2, become the references for the controllers at Level 1.

3.3. Level 1: Local controllers

At this level, primary controllers, which receive the setpoints from the secondary controllers and send control actions to the process actuators are defined. Considering the need for a high-speed actuation and low computation time, a PFC-based (PFC1) control strategy has been chosen to control the O_2 concentration in C4a by adjusting the light intensity. The control law is derived based on the first-order model parameters identified in Alemany et al. (2019) and using (28)-(33) as follows:

$$W(m) = \frac{\left[C_{O_2}^{C4a}|_g^{ref}(m) - C_{O_2}^{C4a}|_g^{p}(m)\right] \cdot lh_{PFC1} + \beta_{m,PFC1} \cdot \hat{C}_{O_2}^{C4a}|_g(m)}{K_{m,PFC1} \cdot \beta_{m,PFC1}} \tag{64}$$

Level 1 is triggered every 36 s (fast clock in Fig. 4) to respond to O_2 fluctuations in the gas outflow of the C4a compartment ($C_{O_2}^{C4a}|_g$). The constraints are related to the lower W^{min} and upper W^{max} bounds of the light intensity. A summary of the proposed HCS is represented in Fig. 4.

4. Simulation results

4.1. Simulation Plan

In this section, the performance of the proposed control method is evaluated using the MELiSSA Pilot Plant as a test case under different operating scenarios. The time interval used for simulation is 120 days. Simulations are conducted in MATLAB environment and Parallel computing Toolbox and Aalborg University cloud service (CLAAUDIA) are employed for parallel computations. Different controller specifications that are considered for the simulations are given in Table 1.

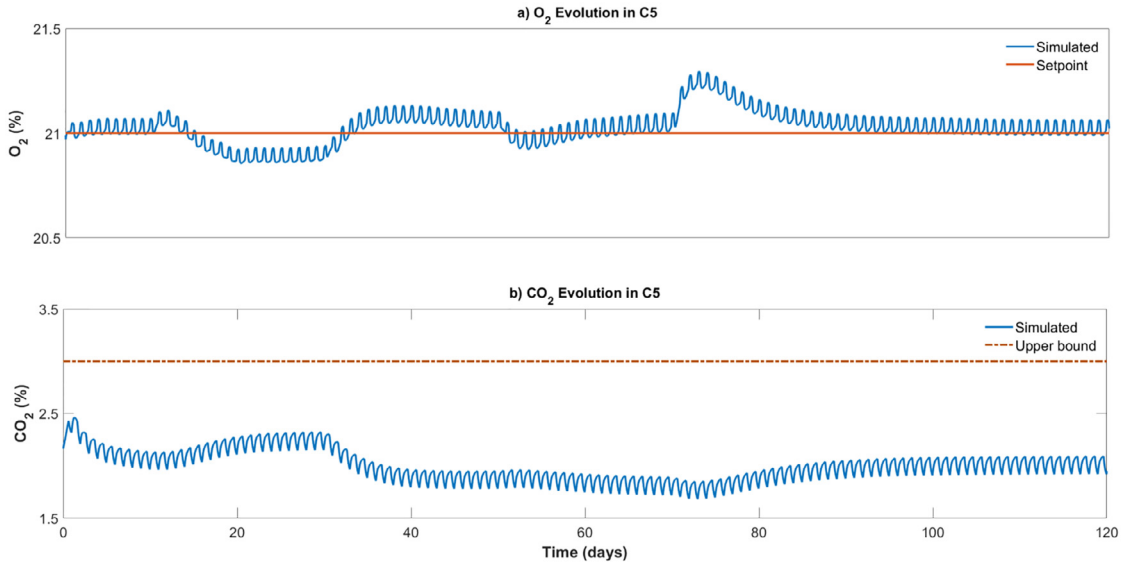

Fig. 5. Evolution of (a) O_2 and (b) CO_2 in the gas phase of C5.

Table 1
Controller's specifications.

Par	Value	Par	Value
$S^{CT,ref}$	0.5	$W^{nom}_{day}/W^{nom}_{night}$	225/84 Wm^{-2}
$S^{CT,min/max}$	0/1	Np_3=$Nc3$	6
W^{min}/W^{max}	10/364 Wm^{-2}	Np_2=Nc_2	5
$G^{CT,min/max}$	$-10/10$ Lh^{-1}	λ_1	5
$P^{CT,max}$	50×10^5Pa	$\lambda_2=\lambda_3$	1
V^{CT}	10L	$\lambda_4,\ldots,\lambda_7$	0.1
$C^{C5}_{O_2\|g}{}^{ref}$	21%	$T_{S,3}$	1h
$C^{C4a}_{O_2\|g}{}^{min/max}$	18/24%	$T_{S,2}$	$0.1T_{S,3}$
$C^{C5}_{O_2\|g}{}^{min/max}$	0/3%	$T_{S,1}$	$0.1T_{S,2}$
$\rho^{min/max}$	0.1/0.9		

As mentioned in Section 3, the parameter identification of the PFC first-order models has been inferred based on the MELiSSA Pilot Plant experimental data, which has also represented a test-bed for the control implementation and large-scale validation. The controller parameters regarding PFC_2 and PFC_1 are listed in Table 2.

The data required for modeling the MELiSSA Pilot Plant can be accessed in Pérez et al. (2005a) for C3 and Alemany et al. (2019) for C4a and C5. A simulation with changing nitrogen load (ammonium load is also used indistinctively) in the input of C3 has been performed. By changing the nitrogen load, the overall demand of O_2 changes, and the response performance of the proposed HCS can be assessed. The details of the simulation schedule are given in Table 3 . As the nitrogen inflow increases/decreases, the required O_2 by C3 ($\hat{D}^{C3}_{O_2}$) to oxidize it, also increases/decreases. The control system is responsible to coordinate all O_2 producer and consumer compartments as well as the concentrated gas tank to satisfy the main requirements of the loop.

4.2. Results

Main Outcome- As the main outcome of the study, Fig. 5a demonstrates that O_2 in the crew compartment is appropriately maintained within the required limits while following the desired reference of 21%.

The reason for this fluctuation, which evolves according to the nitrogen load, lies in the fact that in the secondary controller, the O_2 reference-tracking requirement in C5 defined in (47) is introduced in the optimization problem as a soft constraint. Therefore, deviations from the reference are allowed under a penalization defined by the weight factor λ_3, without violating the limits as defined in (60). From a process point of view, when O_2 demand is high (for example when nitrogen load is at its highest point after 50 days), the concentration of O_2 in C5 decreases. The reason for this behavior is that the optimization problem in Level 3 and Level 2 controllers provide a compromise between the precision of the reference tracking in C5 and the deviation of the operating conditions from the desired nominal operating points defined by parameters $S^{CT,ref}$ and $W^{nom}_{day}/W^{nom}_{night}$ in Table 1. In opposite, when the process operates at its nominal condition, the concentration of O_2 in C5 can track the reference with high precision. In this study, CO_2 is not controlled, but with the operating conditions used, it can be kept below a critical level of 3% as can be seen in Fig. 5b. The already mentioned high degree of coupling between variables makes it necessary to design a CO_2 trap or buffer tank, which introduces a degree of freedom in the system to be able to control CO_2.

Level 3- In Fig. 6, the optimal resource allocation scheduled by solving (34)-(42) is represented. Essentially, Level 3 is constrained by the mass balance in (39) considering a list of technical restrictions and operating criteria. If the process is operating in nominal conditions (Load 1 in Table 3), O_2 is supplied mainly by C4a through adjusting light intensities close to the nominal values. It is important to notice that the oscillations of the system are due to the day-night dynamics of the mock-up crew respiration. During the nighttime, rats consume O_2 and produce CO_2 at a reduced rate in relation to the day shift causing the repeated oscillation observed in most of the variables represented in this section. This is also the reason why two nominal points of light intensity are used in C4a, so that the resource utilization can be optimized. In Fig. 6, it can be observed how the concentrated gas tank is coordinated with C4a to handle the excess and deficit of O_2 in the system. Thus, when the consumption rate of C3 and C5 exceeds C4a production capacity (from 25 to 30 days in Fig. 6b), the concentrated gas tank is mainly discharged (red area in Fig. 6b). On the contrary, if C4a has enough production capacity (from 30 to 38 hr in Fig. 6b), the concentrated gas tank is mainly charged (purple area in Fig. 6b).

Level 2- Once Level 3 has determined the resource allocation in terms of O_2 production rates from C4a and the concentrated gas

Table 2
Predictive functional controllers' parameter.

Name	Control command	Time constant (**h**)	Gain	Coincidence point (h)	Closed loop response time (h)	Reference	HCS level
PFC 2	G_{in}^{C3}	0.01	0.0459	0.1	0.03	$C_{O_2}^{C3}\|_l^{ref}$	2
PFC 1	Light intensity (W)	0.15	0.007% O_2 /W/m^2	0.01	0.45	$C_{O_2}^{C4a}\|_g^{ref}$	1

Table 3
Simulation Schedule.

Step	Inlet Flow (mL/min)	[NH_4] (mg/L)	N Load (mg N L^{-1} day^{-1})	Time Interval (day)
Load1*	20.8	128.6	435	0–10
Load2	16.4	128.6	343	10–30
Load3	27.8	128.6	580	30–50
Load4	33.5	128.6	700	50–70
Load1	20.8	128.6	435	70–120

* Nominal operating condition.

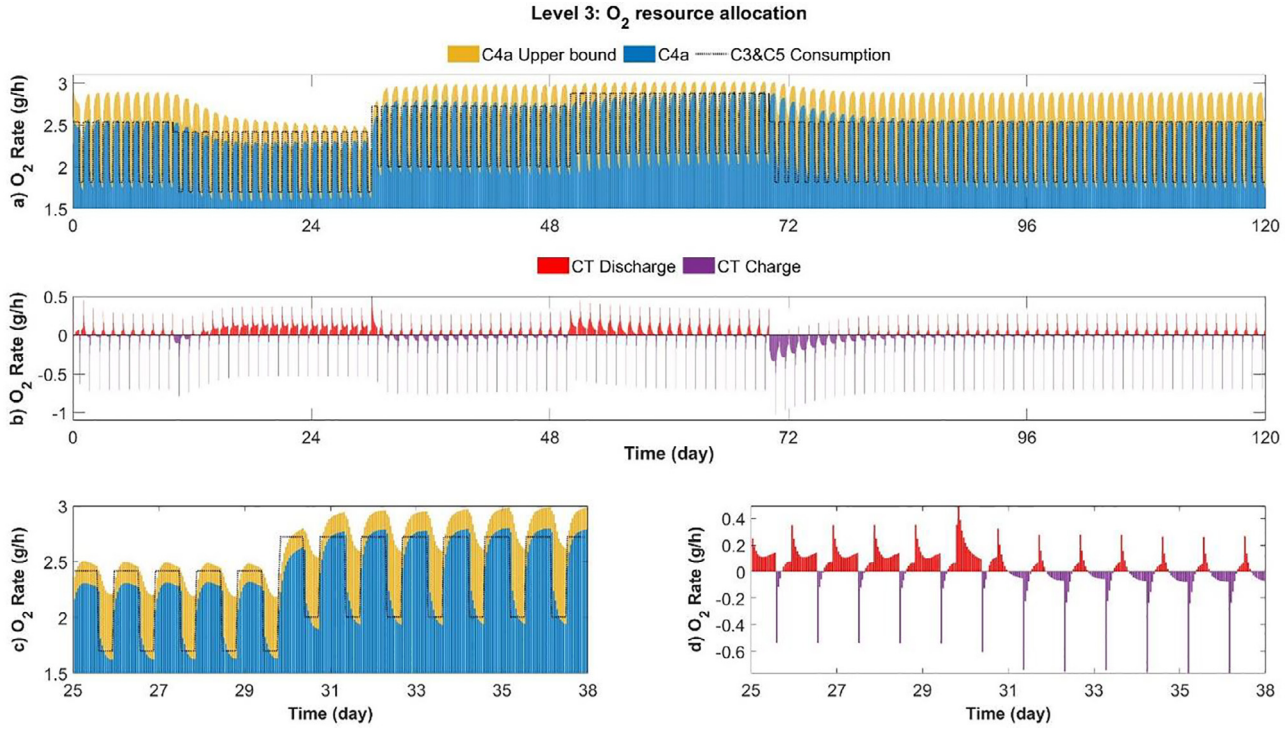

Fig. 6. a) Overall demand of O_2 from C3 and C5 and the optimal resource allocation of C4a; b) Concentrated gas tank charging(-)/discharging(+) rates according to tertiary level decisions; c) and d) are zoomed plots of a) and b) respectively from day 25 to 38.

tank, references are sent to the secondary controller, which generates reference signals to be tracked by local controllers through solving the control problem presented in (46)-(63). In Fig. 7, where the output of the secondary controller is represented, a high performance can be observed in terms of precision in the tracking of the references received from Level 3. PFC2 performance will be assessed in the next section.

4.2.1. Local controllers and process performance

According to Table 3, Load 2 corresponds to the lowest Nitrogen load in C3 which carries the lowest O_2 demand. Nevertheless, it is also observed in Fig. 6b that with this low amount of nitrogen load, the concentrated gas tank needs to be discharged to satisfy the overall O_2 demand. The reason for this apparent contradictory phenomenon about low O_2 demand and discharging of the concentrated gas tank can be explained by the resource limitation in C4a. According to (4)-(8), when the substrate y concentration decreases, the associated limiting factor decreases $\Psi_y^z < 1$, hence, cell growth and productivity of O_2 also decrease. In Fig. 8a, Ψ_y^z is represented for CO_2 and HNO_3, demonstrating that when nitrogen load is decreased in Load 2 scenario, C4a receives less nitrate and its O_2 productivity is threatened. It is also important to highlight that according to Table 3 the concentration of NH_4 in the input of C3 is not changed, but the flow of input liquid (F_{in}^{C3}) is changed. Hence, the concentration of nitrate in the input of C4a is time-invariant, considering that C3 operates at full nitrification. The cause of the limitation is that reducing the flow involves increasing the residence time in the photobioreactor C4a, increasing its biomass concentration (increasing the population) until the consumption rate of nitrate crosses a boundary that implies nitrogen (resource) limitation (see Fig.8b). This is a paradigmatic example of the degree of interdependency between variables involved in biochemical reactions.

The control system proposed in this study can overcome this type of limitation by deploying efficient predictions. The tertiary controller uses the measurements obtained from the plant, which in combination with the internal model presented in Section 2, can anticipate some of the negative phenomena that the process can

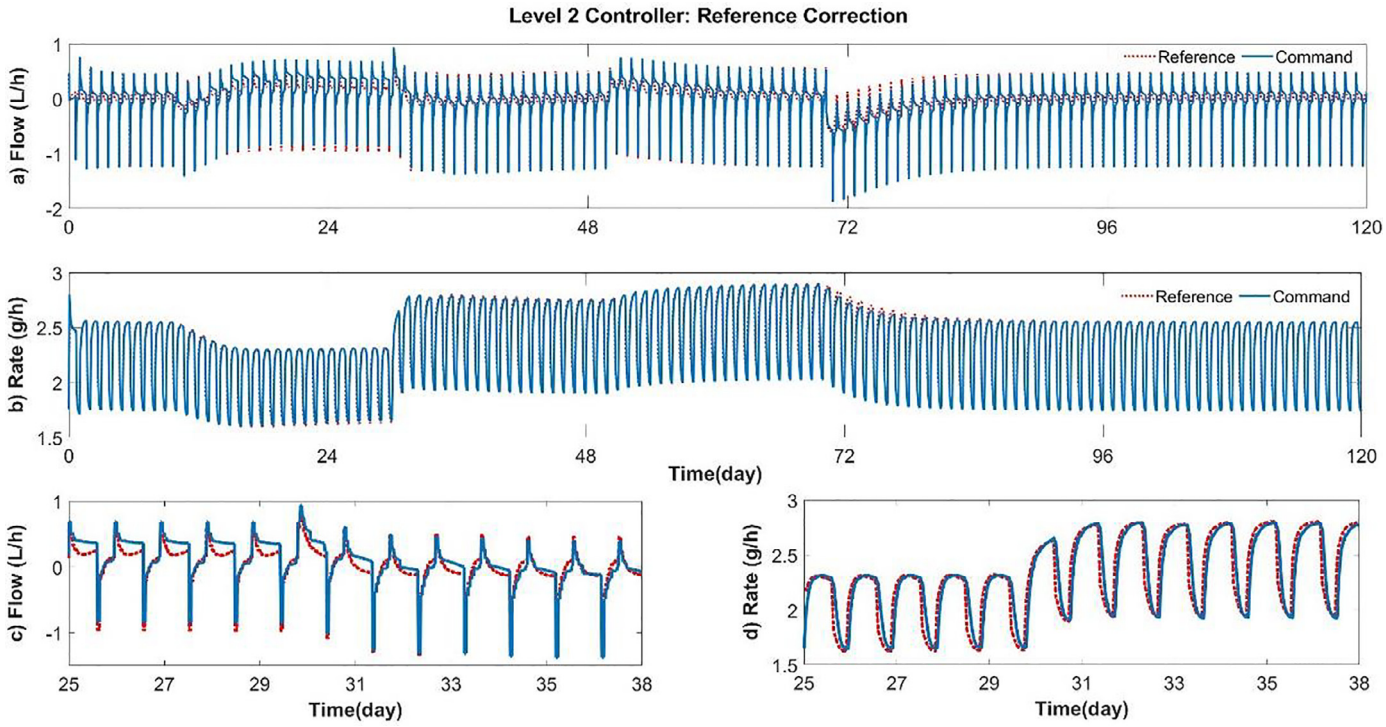

Fig. 7. a) Concentrated gas tank charging (-)/discharging(+) rate; b) Oxygen production rate of C4a; c) and d) are zoomed plots of a) and b) respectively from day 25 to 38.

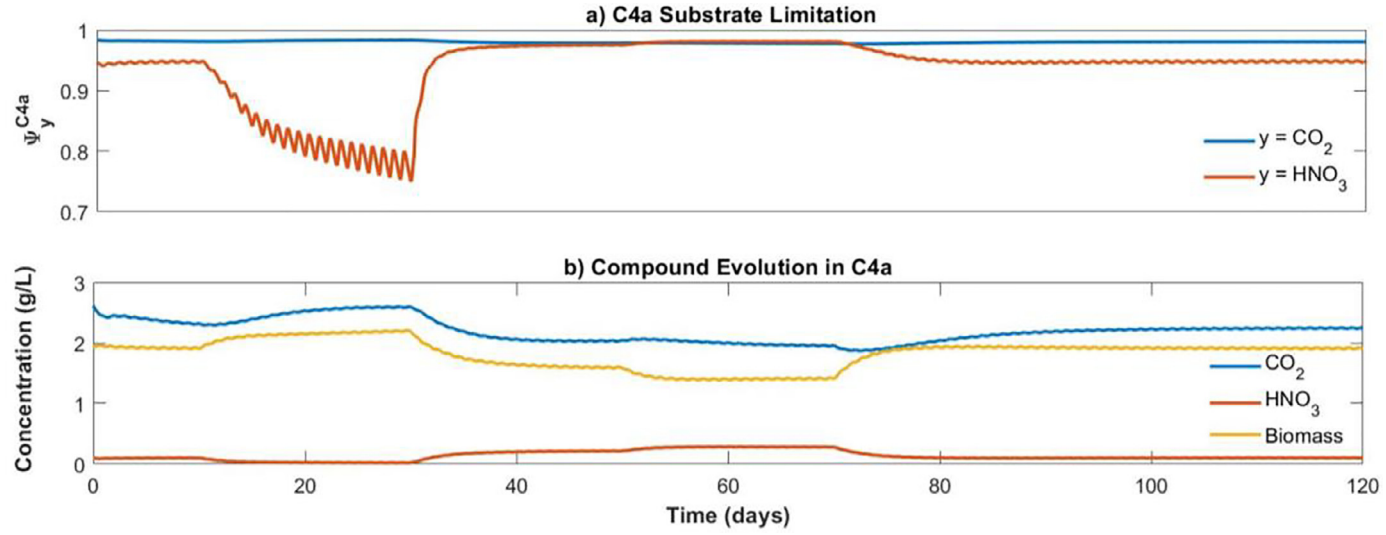

Fig. 8. a) Substrate limitation in C4a associated to Carbon and Nitrogen sources b) Concentration of compounds in the liquid phase in the output of C4a.

face as long as they are properly considered in the internal model. When the nitrogen load is at its highest level (Load 4), it can be observed in Fig. 6b that the concentrated gas tank needs to be discharged, not because of a nitrogen limitation in C4a, but because of the high O_2 demand in the system. At this point, C4a approaches its maximum production capacity, which is penalized by the objective function. As can be observed, the HCS defines an optimal strategy for charging and discharging the concentrated gas tank for compensating, either the default of nitrogen availability or the excess in O_2 demand of the system.

According to the diagram in Fig. 4, the secondary controller requires information about the gas inflow in C3 to be able to generate the rest of the control references. By applying the PFC in (43), the gas flow is determined based on the expected O_2 demand, which is predicted at the tertiary level. Fig. 9a demonstrates that whenever nitrogen load is increased, so does the reference dissolved O_2 in C3 following (45). To track these reference changes, the input gas flow (Fig. 9b) is modified to inject more concentrated O_2 from the membrane separation unit when more nitrogen is loaded in C3. As it can be seen in Fig. 9c, PFC is proven to be very efficient in guaranteeing that no NH_4 is sent to C4a.

Regarding the output of the secondary controller, the concentrated gas tank flow (Fig. 7a) can be directly sent to the local controller, but the O_2 production rate assigned to C4a (Fig. 7b) depends on the C4a gas flow and the O_2 concentration in the output of C4a. Thus, secondary controller determines optimal flows and concentration setpoints to be tracked by the local controllers Given the flow rate generated by Level 2, the control of O_2 concentration in C4a is performed by adjusting the light intensity in the primary controller. As mentioned, the operating criteria for C4a is to

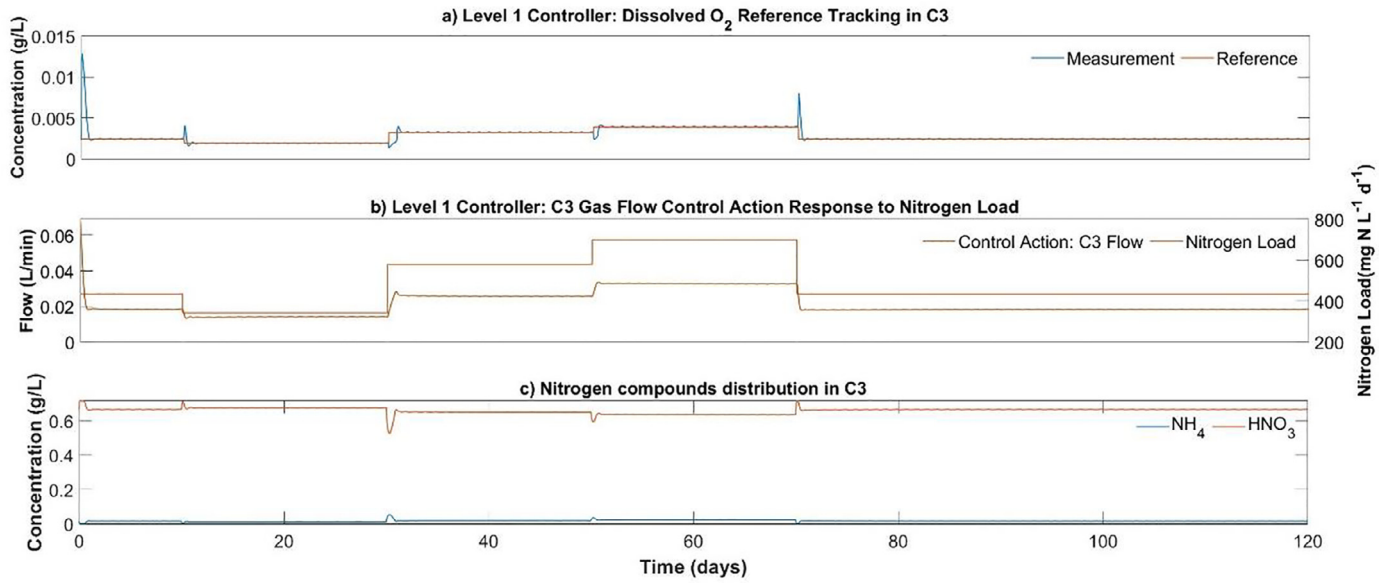

Fig. 9. Summary of oxygen controller in C3. a) Dissolved oxygen tracking to guarantee ammonia oxidization to nitrate b) C3 Gas inflow representation as a control command in response to varying nitrogen load c) Distribution of nitrogen compounds of C3 in the liquid phase.

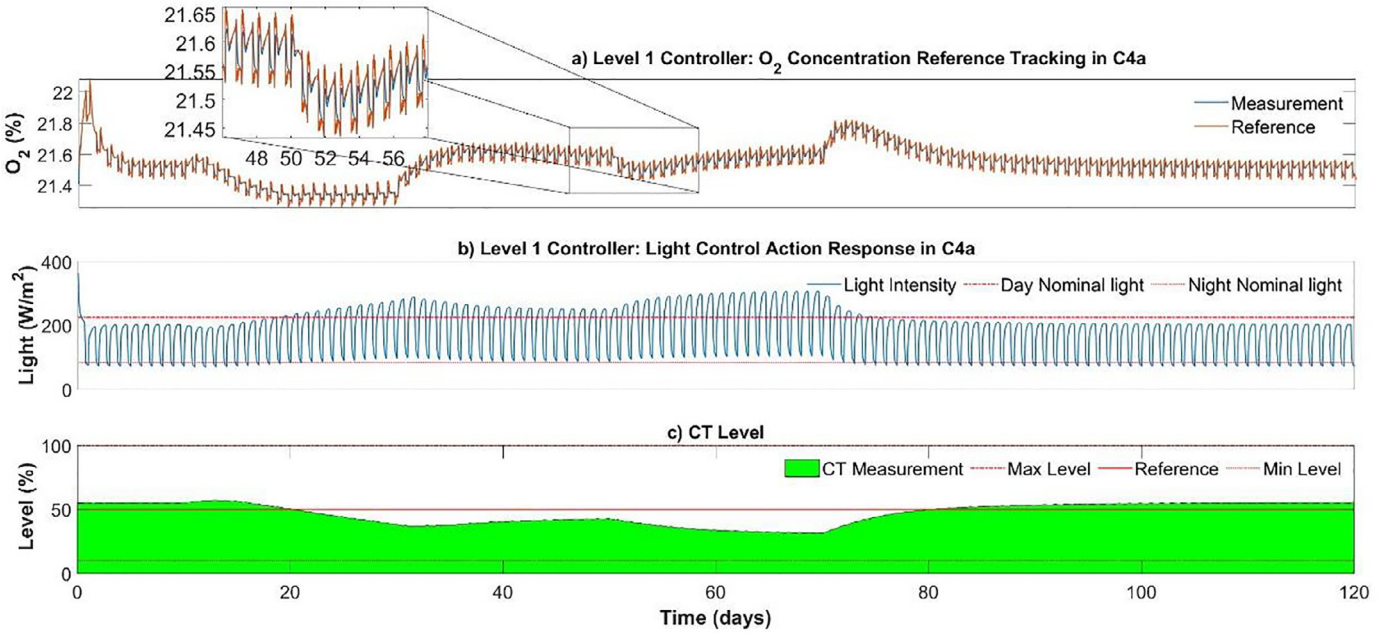

Fig. 10. Performance of the controllers in Level 1: a) Oxygen reference tracking in C4a, b) C4a light adjustment, c) Concentrated gas tank level.

work with two nominal levels of light intensity. In Fig. 10a, it can be observed that the O_2 concentration in C4a follows with good precision the reference received from Level 2. The performance of the PFC controller has been already validated in the MELiSSA Pilot Plant. In Fig. 10b it is shown that when the process operates at the nominal operating condition (Load 1) the light intensity is close to the day and night nominal points (225 and 84 W/m^2 respectively), while in scenarios when different nitrogen loads are applied, light intensity tends to deviate from the nominal levels following the priority given to different objective functions of the secondary controller. Fig. 10c shows the evolution of the concentrated gas tank storage level over the simulation time, tracking the desired reference imposed by the supervisory controller at a value of 50%. As the reference for concentrated gas tank is set to 50%, as soon as the production capacity of C4a can satisfy the overall O_2 demand, the tank is charged to restore its desired level. This is observed in Fig. 10c when the nominal operating conditions are restored from day 70 until the end of the simulation. Hence, the light intensity profile in C4a is never saturated as it stays around the nominal point and similarly, the concentrated gas tank level fluctuates around 50%.

Satisfactory results have been achieved regarding both the operation of the system following the desired references guaranteeing a safe environment for the crew and the achievement of a high degree of resilience to changes. The computational time required at different levels in the proposed HCS is also satisfactory, given the complexity of the MPC used for Levels 3 and 2. Details about the computational cost of different controllers can be found in Table 4.

Table 4
Controllers Computational Cost.

Level in HCS	Maximum (*sec*)	Minimum (*sec*)	Mean (*sec*)
Prediction	122.15	65.74	70.06
Level 3	2.72	0.55	0.62
Level 2	9.38	1.07	2.065
Level 1	<0.1	<0.1	<0.1

5. Future works

In Section 4, the proposed HCS has been applied to an exemplary LSS, MELiSSA Pilot Plant, in MATLAB environment using its well-tested and validated models. According to the results, the proposed controller has a satisfactory performance to achieve the operating goals of the system while satisfying the main requirements determined in LSS standards. It is worth mentioning that, as the main focus of this paper is to demonstrate the potential of a hierarchical control strategy for operation management of a LSS with a variety of constraints and operating goals, analyzing the effects of uncertainty on the controller performance is proposed as an important future research direction. Mitigating model uncertainties and sensor noise caused by the uncertain behavior of the crew are among the main issues that necessitate the deployment of advanced robust and stochastic control strategies. Besides, this paper focuses on the mass balance and oxygen control of the CELSS and only the gas phase loop is considered for a mock-up crew of three rats. Integrating energy and thermal subsystems as well as the liquid phase loop are also of vital importance to have a coordinated framework to control a human-rated regenerative life support systems that will be followed by the authors in their future research.

6. Conclusions

In this paper, HCS and energy management strategies of MGs are extended to control ecological LSSs, which have a very complex nature reflected in the mathematical modeling and present many challenges including non-linearities, interrelated system dynamics, hard constraints, scarce resources, and degrees of freedom, and especially a high degree of variable and functions coupling. All this requires a HCS with different levels to supervise (Supervisory Level), manage (Level 3), adjust (Level 2), and execute (Level 1) control commands. The platform presented will be used in the future to adapt the proposed HCS to further integration steps pursued in the MELiSSA Pilot Plant. Increasing the number of compartments will naturally increase the control complexity. Among others, it will force to include water and edible material production for the crew, to assess the use of buffer elements to ensure optimal control of the plant, as well as to appraise the control architecture resilience and robustness.

Declaration of Competing Interest

The authors declare that they have no known competing financial interests or personal relationships that could have appeared to influence the work reported in this paper.

CRediT authorship contribution statement

Carles Ciurans: Writing – original draft, Writing – review & editing, Conceptualization, Software, Formal analysis. **Najmeh Bazmohammadi:** Writing – original draft, Writing – review & editing, Conceptualization, Software, Methodology. **Laurent Poughon:** Investigation, Resources. **Juan C. Vasquez:** Conceptualization, Methodology, Supervision. **Claude G. Dussap:** Investigation, Resources, Supervision, Funding acquisition. **Francesc Gòdia:** Supervision, Project administration, Funding acquisition. **Josep M. Guerrero:** Conceptualization, Methodology, Supervision, Funding acquisition.

Acknowledgements

This work was supported by VILLUM FONDEN under the VILLUM Investigator Grant (no. 25920): Center for Research on Microgrids (CROM). The MELiSSA Pilot Plant is funded from ESA contributions from Spain (main contributor), Belgium, France, Italy and Norway, under Frame Contract C4000109802/13/NL/CP. Co-funding from Ministerio de Ciencia, Innovación y Universidades, Generalitat de Catalunya and Universitat Autònoma de Barcelona is also acknowledged (https://www.melissafoundation.org)

References

Alemany, L., Peiro, E., Arnau, C., Garcia, D., Poughon, L., Cornet, J.F., Dussap, C.G., Gerbi, O., Lamaze, B., Lasseur, C., Godia, F., 2019. Continuous controlled long-term operation and modeling of a closed loop connecting an air-lift photobioreactor and an animal compartment for the development of a life support system. Biochem. Eng. J. 151. doi:10.1016/j.bej.2019.107323.

Barta, D., 2017. Getting out of orbit: water recycling requirements and technology need for long duration missions away from Earth. In: 20th Annual Nanotech 2017 Conference and Expo, pp. 1–9.

Brunet, J., Gerbi, O., André, P., Davin, E., Avezuela Rodriguez, R., Carbonero, F.O., Soumalainen, E., Lasseur, C., 2010. Alisse : advanced life support system evaluator. In: 38th COSPAR Scientific Assembly, p. 2.

Ciurans, C., Bazmohammadi, N., Vasquez, J.C., Dussap, G., Guerrero, J.M., Godia, F., 2021. Hierarchical control of space closed ecosystems – expanding microgrid concepts to bioastronautics. IEEE Ind. Electron. Mag. 2–13. doi:10.1109/MIE.2020.3026828.

Cornet, J.F.; Dussap, C.G.; Dubertret, G., 1992. A structured model for simulation of cultures of cyanobacterium Spyrulina platensis in Photobioreactors coupling between light transfer and growth kinetics.

Cornet, J.F., Dussap, C.G., Gros, J.B., Binois, C., Lasseur, C., 1995. A simplified monodimensional approach for modeling coupling between radiant light transfer and growth kinetics in photobioreactors. Chem. Eng. Sci. 50, 1489–1500. doi:10.1016/0009-2509(95)00022-W.

Cruvellier, N., Poughon, L., Creuly, C., Dussap, C.G., Lasseur, C., 2017. High ammonium loading and nitrification modelling in a fixed-bed bioreactor. J. Water Process Eng. 20, 90–96. doi:10.1016/j.jwpe.2017.10.006.

Dauchet, J., Cornet, J.F., Gros, F., Roudet, M., Dussap, C.G., 2016. Photobioreactor modeling and radiative transfer analysis for engineering purposes. Adv. Chem. Eng. 48, 1–106. doi:10.1016/bs.ache.2015.11.003.

Ehlmann, B.L., Chowdhury, J., Marzullo, T.C., Eric Collins, R., Litzenberger, J., Ibsen, S., Krauser, W.R., Dekock, B., Hannon, M., Kinnevan, J., Shepard, R., Douglas Grant, F., 2005. Humans to Mars: a feasibility and cost-benefit analysis. Acta Astronaut 56, 851–858. doi:10.1016/j.actaastro.2005.01.010.

European Comission, 2010. Directive 2010/63/EU of the european parliament and the council of 22 September 2010 on the protection of animals used for scientific purposes. Off. J. Eur. Union 1–162.

Gitelson, J., Lisovsky, G., 2002. Man-Made Closed Ecological Systems.

Gòdia, F., Albiol, J., Pérez, J., Creus, N., Cabello, F., Montràs, A., Masot, A., Lasseur, C., 2004. The MELISSA pilot plant facility as an integration test-bed for advanced life support systems. Adv. Sp. Res. 34, 1483–1493. doi:10.1016/j.asr.2003.08.038.

Jones, H., 2003. Design rules for space life support systems. SAE Tech. Pap. doi:10.4271/2003-01-2356.

A.Henson, Michael, 1998. Nonlinear model predictive control current states and future directions.pdf. Comput. Chem. Eng..

NASA, 2019. Nasa Spaceflight Human-System Standard. Volume2: Human Factors, Habitability, and Environmental Health.

Nelson, M., Allen, J., Alling, A., Dempster, W.F., Silverstone, S., 2003. Earth applications of closed ecological systems: relevance to the development of sustainability in our global biosphere. Adv. Sp. Res. 31, 1649–1655. doi:10.1016/S0273-1177(03)80011-X.

Nelson, M., Burgess, T.L., Alling, A., Alvarez-Romo, N., Dempster, W.F., Walford, R.L., Allen, J.P., 1993. Using a closed ecological system to study Earth's biosphere: initial results from Biosphere 2. Bioscience 43, 225–236. doi:10.2307/1312123.

Nelson, M., Pechurkin, N.S., Allen, J.P., Somova, L.A., Gitelson, J.I., 2010. Closed ecological systems, space life support and Biospherics. Environ. Biotechnol doi:10.1007/978-1-60327-140-0_11.

Ocampo-Martinez, C., Barcelli, D., Puig, V., Bemporad, A., 2012. Hierarchical and decentralised model predictive control of drinking water networks: application to Barcelona case study. IET Control Theory Appl 6, 62–71. doi:10.1049/iet-cta.2010.0737.

Olivares, D.E., Canizares, C.A., Kazerani, M., 2014. A centralized energy management system for isolated microgrids. IEEE Trans. Smart Grid 5, 1864–1875. doi:10.1109/TSG.2013.2294187.

Pérez, J., Poughon, L., Dussap, C.G., Montesinos, J.L., Gòdia, F., 2005a. Dynamics and steady state operation of a nitrifying fixed bed biofilm reactor: mathematical

model based description. Process Biochem 40, 2359–2369. doi:10.1016/j.procbio.2004.09.022.

Pérez, J., Poughon, L., Dussap, C.G., Montesinos, J.L., Gòdia, F., 2005b. Dynamics and steady state operation of a nitrifying fixed bed biofilm reactor: mathematical model based description. Process Biochem 40, 2359–2369. doi:10.1016/j.procbio.2004.09.022.

Poughon, L., Dussap, C.G., Gros, J.B., 1999. Dynamic model of a nitrifying fixed bed column: simulation of the biomass distribution of Nitrosomonas and Nitrobacter and of transient behaviour of the column. Bioprocess Eng 20, 209–221. doi:10.1007/s004490050583.

Richalet, J., 1993. Practique De La Commande Predictive. Hermes Sciences Publicat.

Schwartzkopf, S.H., 1992. Design of a controlled ecological life support system: regenerative technologies are necessary for implementation in a lunar base CELSS. Bioscience 42, 526–535. doi:10.2307/1311883.

Sulzman, F.M., 1994. Life Support and Habitability. Vol II. Space Biology and Medicine.

Vasquez, J., Guerrero, J., Miret, J., Castilla, M., De Vicuña, L., 2010. Hierarchical control of intelligent Microgrids. IEEE Ind. Electron. Mag. 23–29.